JOURNAL OF VIROLOGY, May 2009, p. 4912–4922 Vol. 83, No. 10
0022-538X/09/$08.00+0 doi:10.1128/JVI.02343-08

Neurodegeneration Induced by PVC-211 Murine Leukemia Virus Is Associated with Increased Levels of Vascular Endothelial Growth Factor and Macrophage Inflammatory Protein 1α and Is Inhibited by Blocking Activation of Microglia▽

Xiujie Li, Charlotte Hanson, Joan L. Cmarik, and Sandra Ruscetti*

Laboratory of Cancer Prevention, National Cancer Institute—Frederick, Frederick, Maryland 21702

Received 10 November 2008/Accepted 28 February 2009

PVC-211 murine leukemia virus (MuLV) is a neuropathogenic retrovirus that has undergone genetic changes from its nonneuropathogenic parent, Friend MuLV, that allow it to efficiently infect rat brain capillary endothelial cells (BCEC). To clarify the mechanism by which PVC-211 MuLV expression in BCEC induces neurological disease, we examined virus-infected rats at various times during neurological disease progression for vascular and inflammatory changes. As early as 2 weeks after virus infection and before any marked appearance of spongiform neurodegeneration, we detected vessel leakage and an increase in size and number of vessels in the areas of the brain that eventually become diseased. Consistent with these findings, the amount of vascular endothelial growth factor (VEGF) increased in the brain as early as 1 to 2 weeks postinfection. Also detected at this early disease stage was an increased level of macrophage inflammatory protein 1α (MIP-1α), a cytokine involved in recruitment of microglia to the brain. This was followed at 3 weeks postinfection by a marked accumulation of activated microglia in the spongiform areas of the brain accompanied by an increase in tissue plasminogen activator, a product of microglia implicated in neurodegeneration. Pathological observations at the end stage of the disease included loss of neurons, decreased myelination, and mild muscle atrophy. Treatment of PVC-211 MuLV-infected rats with clodronate-containing liposomes, which specifically kill microglia, significantly blocked neurodegeneration. Together, these results suggest that PVC-211 MuLV infection of BCEC results in the production of VEGF and MIP-1α, leading to the vascular changes and microglial activation necessary to cause neurodegeneration.

PVC-211 murine leukemia virus (MuLV), a highly neuropathogenic variant of the leukemia-inducing virus Friend MuLV (F-MuLV), induces a rapid, age-dependent spongiform neurodegenerative disease in rodents, resulting in paralysis (24, 33). The primary target of PVC-211 MuLV infection within the rat central nervous system (CNS) is brain capillary endothelial cells (BCEC), which are resistant to F-MuLV infection (19). Previous studies using chimeras between PVC-211 MuLV and F-MuLV demonstrated that infection of BCEC is a prerequisite for neurodegeneration induced by PVC-211 MuLV (32). Further studies attributed the ability of PVC-211 MuLV to efficiently infect BCEC to two amino acid changes in the receptor binding domain of its envelope protein (31), which creates a unique heparin binding domain that may allow the virus to bind to proteoglycans on the surface of BCEC (22), aiding infection of this difficult-to-infect cell type. These results suggested that neurodegeneration caused by PVC-211 MuLV is an indirect result of virus infection of blood vessels within the CNS.

The spongiform vacuolation observed in PVC-211 MuLV-infected brains is associated with oxidative damage (47), and BCEC isolated from PVC-211 MuLV-infected rats produce inducible nitric oxide synthase (iNOS) (23). However, iNOS was not induced after in vitro infection of primary BCEC, suggesting that expression of the virus in BCEC is insufficient to activate iNOS. Activated microglia, which can be detected in the brains of PVC-211 MuLV-infected rats (47), release inflammatory molecules that are known mediators of iNOS induction, and these molecules may stimulate BCEC to express iNOS and other factors. Microglial activation is thought to play a role in neuron death in a number of diseases (6, 26). Unlike BCEC, microglia in PVC-211 MuLV-infected brains are not infected with the virus, so the mechanism by which microglia are activated is unclear. Since vascular damage has been shown to lead to microglial activation (11), it is possible that PVC-211 MuLV infection of BCEC results in damaged vessels, causing the activation of microglia. Although an earlier study failed to detect enough vessel damage in the brains of PVC-211 MuLV-infected rats to allow entry of horseradish peroxidase across the blood-brain barrier (19), one cannot rule out the possibility that the virus causes more subtle vessel damage that is still sufficient to activate microglia.

In this study, we examined the brains of rats at various times after infection with PVC-211 MuLV and found that vascular and inflammatory changes, associated with elevation of the endothelial cell growth factor VEGF and the inflammatory chemokine MIP-1α, occur early in the course of the disease. After spongiform neurodegeneration occurred, we detected loss of neurons, demyelination, axonal degeneration, and muscle atrophy as well as high levels of tissue plasminogen activator (tPA). Treatment of rats with clodronate-containing lipo-

* Corresponding author. Mailing address: Laboratory of Cancer Prevention, Building 567, Room 152, National Cancer Institute—Frederick, Frederick, MD 21702-1201. Phone: (301) 846-5740. Fax: (301) 846-6164. E-mail: ruscetti@ncifcrf.gov.

▽ Published ahead of print on 11 March 2009.

somes, which specifically kill macrophages and microglia, blocked the development of PVC-211 MuLV-induced neurodegeneration.

MATERIALS AND METHODS

Virus and animals. Neuropathogenic PVC-211 MuLV and its nonneuropathogenic variant PVFe5 MuLV were grown in Rat-1 or NIH 3T3 fibroblasts in Dulbecco's minimal essential medium (DMEM) plus 10% fetal calf serum (FCS) as previously described (31). Virus samples were collected after 24-h incubation of cells with fresh medium and stored at −80°C until use. Pregnant Fisher 344 (F344) rats were obtained from the Small Animal Facility at the National Cancer Institute—Frederick. Two-day-old F344 rats were inoculated intracranially (i.c.) with 0.05 to 0.075 ml of supernatant from virus-producing cells or with medium.

Virus infection of primary BCEC. Primary rat BCEC were isolated, cultured, and infected with virus as described previously (23). Briefly, cells were rinsed three times in phosphate-buffered saline (PBS) to remove heparin and pretreated for 30 min with DMEM containing 10% FCS and 5 μg/ml of Polybrene. This medium was replaced with virus and Polybrene. After 3 h of incubation, virus was removed and replaced with endothelial cell medium (MEM with D-valine [HyClone, Logan, UT], supplemented with 20% FCS, 1 mM MEM nonessential amino acids, 1 mM vitamin solution, 50 μg/ml of endothelial mitogen [Biomedical Technology Inc., Stoughton, MA], and 16 U/ml of heparin). Medium was changed as needed. Nine days after infection, medium was aspirated and replaced with fresh medium, which was collected 24 h later for further analysis.

Tissue sampling. Rats injected with PVC-211 MuLV or DMEM were euthanized either with avertin (300 mg/kg intraperitoneally [i.p.]) or with CO_2 at 7 and 14 days postinjection (dpi) or when paralyzed (21 to 24 dpi). The collection and preparation of tissues depended upon the experiment to be performed. For histological analysis and immunostaining, rats euthanized with avertin were perfused with 4% paraformaldehyde solution, and then brains were fixed in 10% formaldehyde before being embedded in paraffin. In some cases, fresh brains were collected from rats euthanized with CO_2 and frozen in Tissue-Tek optimal-cutting-temperature (OCT) embedding medium (Sakura Finetek, Torrance, CA). For histological analysis, tissues were cut into 5- to 8-μm sections and kept either at room temperature (RT) for paraffin sections or at −80°C for frozen sections until used. For detection of RNA and protein, fresh tissues, including cerebellum, brain stem, and cortex, as well as serum were collected from rats euthanized with CO_2. The tissues were cut into small pieces and snap-frozen in liquid nitrogen. Tissues and serum were stored at −80°C until needed.

Histology and Immunofluorescence. For histological analysis, paraffin or frozen sections were stained with hematoxylin and eosin (H&E). To identify neurons, slides from paraffin sections of brains (two from each animal) were stained in 1% cresyl violet (Sigma-Aldrich, St. Louis, MO) in formaldehyde. For the cerebellum, all purple-blue-stained cells were counted under a magnification of ×20. For the brain stem, several different fields were counted (×20): two in the medulla oblongata close to the fourth ventricle, one in the midbrain, and one in the pons. For myelin and axon visualization, paraffin sections were stained with luxol fast blue (Solvent Blue 38; Sigma-Aldrich). Slides were visualized under light microscopy. For immunostaining to detect CD31 (PECAM-1) or ED-1, frozen sections were fixed in 50% acetone and 50% methanol at −20°C for 30 min and then permeabilized in 0.3% Triton X–100 PBS for 10 min. After incubation in 5% milk in PBS for 1 h at RT, the slides were incubated overnight at 4°C with either mouse anti-CD31 (1:10, clone TLD-3A12; Pharmingen, San Diego, CA) or mouse anti-ED1 (1:50, MCA341GA; Serotec, Raleigh, NC). The next morning, the slides were washed with PBS and then incubated either with biotinylated anti-mouse immunoglobulin G (IgG) and streptavidin coupled to Alexa Fluor 546 (Molecular Probes, Eugene, OR) for anti-CD31 detection or with goat anti-mouse IgG coupled to Alexa Fluor 488 (Molecular Probes) for anti-ED-1 detection. Similar procedures were carried out for immunostaining to detect MuLV gp70 and neuron-specific enolase (NSE) in paraffin sections. Briefly, the sections were deparaffinized, rehydrated, and then microwaved up to 85°C in 10 mM sodium citrate, pH 6.5. For anti-MuLV gp70 staining, the slides were incubated in 5% normal donkey serum in PBS and then stained with goat anti-Rauscher MuLV gp70 (1 μg/ml; National Cancer Institute, Bethesda, MD) overnight at RT. They were then incubated with donkey anti-goat IgG coupled to Alexa Fluor 568 (Molecular Probes). For anti-NSE staining, the slides were incubated in 2% normal goat serum in PBS and then stained with mouse anti-human NSE (Dakocytomation, Carpinteria, CA) overnight at RT. They were then incubated with goat anti-mouse IgG coupled to Alexa Fluor 488 (Molecular Probes). After three washes in PBS, coverslips were applied to slides with ProLongGold antifade reagent and DAPI (P36931; Invitrogen, Carlsbad, CA). All immunostained sections were analyzed by fluorescence microscopy.

EB analysis. To determine vessel integrity, Evans blue (EB; Sigma-Aldrich) was injected i.p. at a dose of 20 μl/10 g body weight based on a previous study (27). In brief, rats were perfused with 0.5% formaldehyde after the EB injection. Brains and livers were collected, dried, and extracted with formamide. The amount of EB extracted was determined spectrophotometrically by absorbance at 610 nm, and the final amount of EB per milligram of dried tissue was calculated. To detect EB in histological sections of brain tissue, the brain was excised, frozen in OCT, and cut into 10-μm sections. Red EB fluorescence was observed under a fluorescent microscope.

Labeling of vessels with lectin-FITC and calculation of vessel number and size. Rats injected with PVC-211 MuLV or DMEM were euthanized with avertin (300 mg/kg i.p.). Using a 26-gauge needle, a total of 100 μl lectin-FITC (fluorescein isothiocyanate) (FL-1171, 1 μg/μl in PBS; Vector Laboratories, Southfield, MI) was slowly (2 min) injected into the left ventricles of the rats while the heart was beating. The rats were then perfused with a 0.5% paraformaldehyde solution for 5 to 10 min. Brains were collected and frozen in Tissue-Tek OCT medium and then cut into 20-μm sections for immunofluorescence analysis. To determine the number of vessels and vessel diameter, images were analyzed using Image-Pro Plus v6.2 (Media Cybernetics, Bethesda, MD). Vessels were segmented using color and morphological thresholds. The number of positive pixels was counted to determine the vessel area. Vessel diameter was calculated from the same vessel segmentation. Each vessel was divided into segments along its length. The vessel diameter was measured for each segment, and the mean vessel diameter was calculated.

Measurement of VEGF and other cytokine and chemokine proteins. The levels of VEGF protein in brain tissues and in cell supernatants from in vitro-cultured BCEC were determined with the Quantikine mouse VEGF immunoassay kit (catalog no. MMV00; R&D Systems, Minneapolis, MN). The amount of VEGF in tissues was normalized to the protein concentration of tissue lysate, while the amount of VEGF in supernatants from in vitro-cultured BCEC was normalized to the amount of protein recovered from lysates of the corresponding pellets. Protein concentration was measured using a Bio-Rad protein assay (Bio-Rad Laboratories, Hercules, CA). To screen for other cytokines and chemokines, frozen brain tissues from control and virus-infected rats were homogenized in PBS plus 1% bovine serum albumin and 0.1% sodium azide and simultaneously screened for expression of 13 different cytokines and chemokines (see Results) using an enzyme-linked immunosorbent assay (ELISA)-based bead multiplex immunoassay (Biosource International, Camarillo, CA) in conjunction with a Luminex 100 analyzer. The level of MIP-1α in serum was further determined using a CCL3 immunoassay kit (catalog no. MMA00; R&D Systems). To detect MIP-1α in brain tissue, frozen tissues were homogenized in PBS followed by a standardized sandwich ELISA technique as previously described (1, 5) with the following modifications. ELISA microplates (Maxisorp catalog no. 439454; Nalge Nunc International, Rochester, NY) were coated with anti-mouse MIP-1α capture antibody (catalog no. AF-450-NA; R&D Systems) at a dilution of 3 μg/ml in coating buffer (catalog no. 6245; Immunochemistry Technologies, LLC, Bloomington, MN) overnight at RT. Biotinylated anti-mouse MIP-α (3.5 μg/ml; catalog no. BAF450; R&D Systems) was used as a detection antibody. Equal volumes of color reagents A and B were added, followed by the addition of stop solution (catalog no. MMA00; R&D Systems) 30 min later. Recombinant mouse MIP-1α (catalog no. 450-MA; R&D Systems) was used to generate the standard curve from which the concentrations present in the samples were determined. Optical density of each well at 450 nm was obtained using a microplate reader.

Measurement of VEGF and MIP-1α mRNA. Total RNA was isolated from tissues using Trizol (Invitrogen) and 1 μg RNA was added to real-time PCRs, as described previously (27). Quantitative real-time PCR amplification was performed in triplicate with cDNA and primers in combination with SYBR green (SYBR green 2× mix; Atila Biosystems, Palo Alto, CA) on a MyiQ single-color real-time PCR machine (Bio-Rad). The following primer sets were used for amplifications: for VEGF, 5′-CTGTACCTCCACCATGCCAA-3′ (sense) and 5′-ATCGGGGTACTCCTGGAAG-3′ (antisense); for MIP-1α, 5′-CTGCCCTTGCTGTTCTTCTC-3′ (sense) and 5′-CGGTTTCTCTTGGTCAGGAA-3′ (antisense). All PCR protocols included a 3-min polymerase activation step followed by 45 cycles consisting of a 95°C denaturation step for 30 s, annealing at 60°C for 30 s, and an elongation step at 72°C for 30 s. A negative control without template was included for each PCR analysis. Results were normalized according to the average amount of the endogenous hypoxanthine guanine phosphoribosyl transferase gene using the primers 5′-GGCGAGATGAAAGGTTCTGCTA-3′ (S) and 5′-CACACTGGAGAATCAGGCAATG-3′ (AS). Data were collected and analyzed with the provided application software.

Immune precipitation and Western blot analysis. For analysis of MuLV gp70 expression in cell supernatants from virus-infected BCEC, 2 ml of medium was collected after 24 h and immunoprecipitated overnight at 4°C with 1 μg of goat anti-RLV gp70 serum (National Cancer Institute, Bethesda, MD) and subsequently incubated with protein G (Millipore, Temecula, CA) for 1 h. After centrifugation, the pellets were rinsed three times in lysis buffer (1% Triton X-100, 0.5% sodium deoxycholate, 0.1% sodium dodecyl sulfate in PBS) and then resuspended in sodium dodecyl sulfate-polyacrylamide gel electrophoresis sample buffer (Bio-Rad) containing reducing agent. Proteins were separated by electrophoresis on an 8% Tris-glycine gel (Invitrogen) and then transferred to a nitrocellulose membrane (Invitrogen). The membrane was then incubated with anti-RLV gp70 serum as previously described (23). Bound antibody was detected using peroxidase-labeled secondary antibody and an enhanced chemiluminescence system (GE Healthcare, Buckinghamshire, United Kingdom). For analysis of MuLV gp70 and tPA levels in brain tissues, lysates were prepared by resuspending frozen tissues in lysis buffer (1% Triton X-100, 0.5% sodium deoxycholate, 0.1% sodium dodecyl sulfate in PBS supplemented with a 1× protease inhibitor cocktail set [Calbiochem, La Jolla, CA] and 5 mM sodium orthovanadate). After homogenization on ice for 20 min, protein concentrations of the clarified lysates were estimated using a Bio-Rad protein assay (Bio-Rad Laboratories). Proteins were separated by electrophoresis on 10% Tris-glycine gels (Invitrogen) under reducing (for MuLV gp70) or nonreducing (for tPA) conditions and then transferred to nitrocellulose membranes (Invitrogen). The membrane was then incubated with either anti-RLV gp70 serum, anti-tPA (IH6C5; Innovative Research, Southfield, MI), or anti-β-tubulin (Sigma-Aldrich). Bound antibodies were detected with peroxidase-labeled secondary antibodies and the enhanced chemiluminescence system (GE Healthcare).

Preparation of liposomal encapsulated clodronate and depletion of microglia. Multilamellar liposomes were prepared as previously described (15, 45). Phosphatidylcholine (86 mg; Sigma-Aldrich) and cholesterol (8 mg; Sigma-Aldrich) were dissolved in 10 ml chloroform in a 500-ml round-bottom flask and then dried in vacuo on a rotary evaporator to form a film. The film was dispersed by gentle rotation in 10 ml of PBS or 10 ml PBS containing 1.73 g (0.6 M) dichloromethylenediphosphonic acid disodium salt (clodronate, catalog no. D4434; Sigma-Aldrich). The preparations were then kept in argon gas at RT for 2 h. After sonication in a water bath at RT for 3 min, the preparations were kept in argon gas at RT for another 2 h. The liposomes were centrifuged at 100,000 × *g* for 30 min and resuspended in 4 ml PBS. For depletion of microglia, newborn rats received i.c. injections of clodronate-containing liposomes or PBS-containing liposomes on days −1 (75 μl), 2 (100 μl), and 5 (100 μl) after injection of PVC-211 MuLV.

Statistics. Student's paired *t* test was employed for all experiments except for those whose results are shown in Fig. 4C, where both the *t* test and the F test were employed. *P* values less than 0.05 were considered statistically significant. Curve fit analysis and correlation coefficients were determined with Kaleidagraph software (Synergy Software, Reading, PA).

RESULTS

Morphologically abnormal and leaky vessels can be observed in the diseased area of the brains of PVC-211 MuLV-infected rats. Previous studies have shown that within the CNS, PVC-211 MuLV is primarily expressed in BCEC (19) and that BCEC tropism is essential for neuropathogenicity (32). To determine whether vessels in PVC-211 MuLV-infected brains had undergone any changes, we first carried out immunofluorescence on brain sections with an antibody to CD31, which identifies vessels. At 7 dpi, there were no detectable differences between control and virus-infected vessels (data not shown), but by 14 dpi (Fig. 1A), we could detect a large number of vessels in the cerebellums and brain stems of PVC-211 MuLV-infected rats that looked abnormal. This was further confirmed by lectin perfusion to label all vessels (21) (Fig. 1B). Increased numbers ($P < 0.05$) and sizes ($P < 0.05$) of vessels were observed in the cerebellums and brain stems of rats infected with PVC-211 MuLV compared to controls (Fig. 1C), suggesting ongoing vessel remodeling. Interestingly, vessel changes were particularly found in the regions of the brain that were shown to be rich in spongiform neurodegeneration later in the course of disease. Fewer vessel changes were observed at 24 dpi than at 14 dpi in brain sections from PVC-211 MuLV-infected rats (data not shown).

To determine if the vessels from the brains of PVC-211 MuLV-infected rats were leaky like most remodeling vessels, PVC-211 MuLV and control rats were injected with EB at various time points after infection, and their whole brains and livers were extracted with formamide and tested for the presence of EB. As shown in Fig. 2A, the brains of PVC-211 MuLV-infected rats had significantly increased amounts of EB at 14 dpi compared with brains of control rats ($P < 0.05$). No difference between virus-infected and control brains was found at 7 dpi, and the difference at 24 dpi was not significant ($P > 0.05$). No differences in EB levels were found at any time point between virus-infected and control livers, a nondiseased organ. The leaking EB in the brains from PVC-211 MuLV-infected rats was confirmed by fluorescence analysis of the organs (Fig. 2B). These data suggest that the vessels in the diseased areas of PVC-211 MuLV-infected rats are abnormal and leaky.

Increased VEGF was detected at 14 dpi in the cerebellums of rats infected with PVC-211 MuLV in vivo as well as in BCEC infected with PVC-211 MuLV in vitro. Since VEGF is known to increase the permeability of blood vessels, we examined the brains of PVC-211 MuLV infected rats for changes in VEGF expression using a specific ELISA. As shown in Fig. 3A, the cerebellums of PVC-211 MuLV-infected rats expressed almost threefold-higher VEGF levels than those of controls at 14 dpi ($P < 0.05$), with the levels returning to normal or below normal at 24 dpi. No changes in VEGF levels were detected in nondiseased areas of the brains, such as the cerebral cortex, or in livers, which were nondiseased (data not shown). Furthermore, real-time PCR analysis showed higher VEGF RNA expression in the cerebellums from rats infected with PVC-211 MuLV than those of controls at 14 dpi (Fig. 3B) ($P < 0.05$). Since capillary vessels in the brain are the main targets of PVC-211 MuLV and the vessels are abnormal, we were interested in determining whether the virus can directly activate VEGF in primary BCEC after in vitro infection. We therefore infected primary BCEC cultures with PVC-211 MuLV and after 10 days analyzed the culture supernatants for expression of the viral envelope protein and VEGF. As a control, we also infected BCEC with a nonpathogenic variant of PVC-211 MuLV, PVFe5, which grows to high titers in BCEC in vitro. The supernatants from both PVC-211 MuLV- and PVFe5-infected BCEC contained abundant viral gp70 envelope protein (Fig. 3C). Supernatants from PVC-211 MuLV-infected BCEC contained more than twice as much VEGF as supernatants from uninfected or PVFe5-infected BCEC ($P < 0.05$).

The chemokine MIP-1α is specifically elevated in the brains and serum of rats infected 14 days earlier with PVC-211 MuLV, followed by robust microglial activation at 21 dpi and an accumulation of tPA. Based on our observations of abnormal vessels in the brains of PVC-211 MuLV-infected rats as well as a previous report showing activation of microglia (47), we sought to determine whether elevated levels of cytokines or chemokines, in particular those secreted from endothelial cells or microglia, are expressed in the brains of PVC-211 MuLV-infected rats. Therefore, brain tissue (cerebellum and brain stem) from virus-infected and control rats was simultaneously

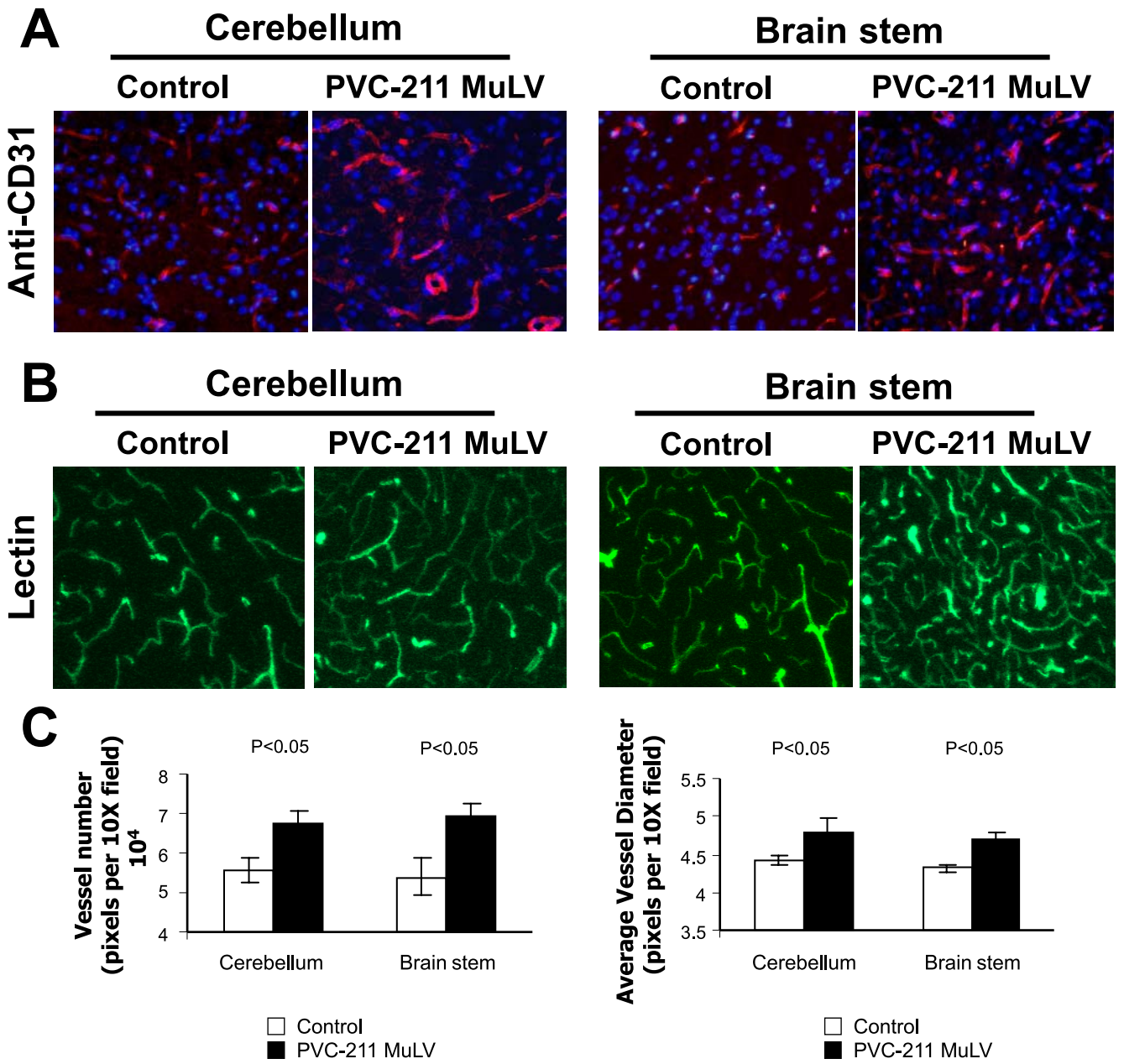

FIG. 1. Vascular changes found at 14 dpi in the diseased areas of the brains of rats infected with PVC-211 MuLV. Brain tissues from rats injected as newborns 14 days previously with PVC-211 MuLV were compared with control rats injected with tissue culture medium. (A) Immunofluorescence with anti-CD31 antibody was performed with brain sections from the cerebellum and brain stem. CD31 staining (red) indicates larger numbers of vessels and increased vessel size in rats infected with PVC-211 MuLV compared to controls. Nuclei are counterstained with DAPI (blue). Magnification, ×20. (B) Lectin labeling (green) of vessels. magnification, ×20. (C) The number of vessels in the cerebellum and brain stem of lectin-stained control and PVC-211 MuLV-infected rats as well as the average diameter of each vessel was determined and plotted. Five animals were used for each group, and each experiment was repeated twice. Results of a representative experiment are shown. Sections used for CD-31 staining and lectin labeling were derived from different animals.

screened for 13 different cytokines and chemokines (MCP-1, MIP-1α, interleukin 1α [IL-1α], IL-1β, IL-2, IL-4, IL-5, IL-6, IL-10, IL-12p40, tumor necrosis factor alpha [TNF-α], gamma interferon, and granulocyte-macrophage colony-stimulating factor) by an ELISA-based bead multiplex assay using Luminex technology (data not shown). This preliminary screen indicated that brain tissue from PVC-211 MuLV-infected rats expressed elevated levels of only one of these factors early in the course of disease: the proinflammatory chemokine MIP-1α, which was higher in the cerebellums and brain stems of PVC-211 MuLV-infected rats than in the controls at 14 dpi but returned to normal by 21 dpi. To confirm the MIP-1α results, a specific ELISA was carried out on serum from control and virus-infected rats. As shown in Fig. 4A, high levels of MIP-1α were clearly detected in the serum of PVC-211 MuLV-infected rats compared with controls. Elevated levels of MIP-1α could

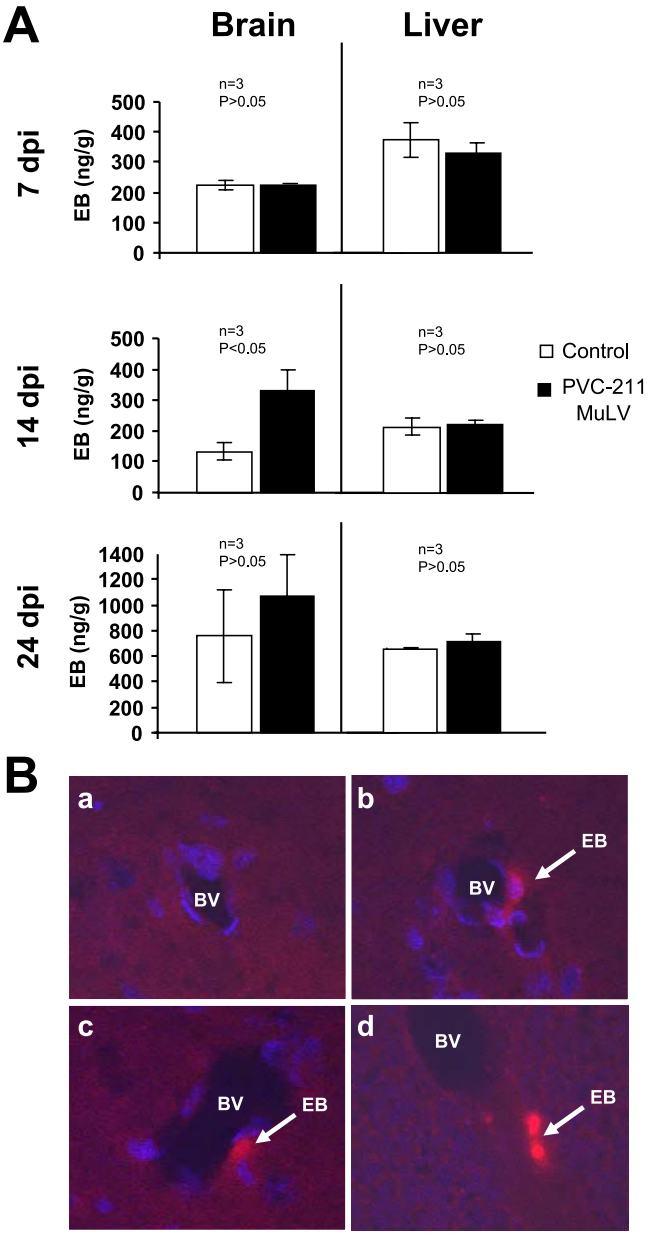

FIG. 2. Leakage of vessels was detected by EB in the brains of rats infected 14 days previously with PVC-211 MuLV. EB was injected into rats treated 7 to 24 days previously with PVC-211 MuLV or medium. Three rats were used for each group, and each experiment was repeated two times, for a total of nine control and nine virus-infected rats. (A) EB was extracted by formamide from whole brains and livers and the levels measured as described in Materials and Methods. A representative experiment is shown. Data are means ± standard errors of the means. (B) Sections of brain stem (a to c) or cerebellum (d) from control rats (a) or PVC-211 MuLV-infected rats (b to d) 14 dpi were examined for EB fluorescence (red) under a fluorescent microscope. The samples used for panels b to d are from different PVC-211 MuLV-infected animals. BV, blood vessel. Nuclei are counterstained with DAPI (blue). Magnification, ×20.

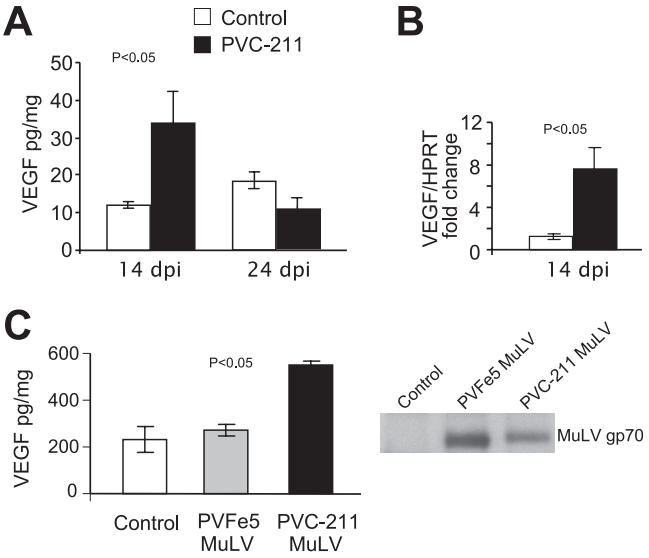

FIG. 3. Increased VEGF protein and RNA were detected at 14 dpi in the cerebellum of rats infected with PVC-211 MuLV in vivo as well as in BCEC infected with PVC-211 MuLV in vitro. (A) Protein levels of VEGF were measured by ELISA in tissues from the cerebellum of rats infected with PVC-211 MuLV or medium. Three animals were used for each group, and each experiment was repeated at least twice. Results of a representative experiment are shown. (B) mRNA levels of VEGF were measured by real-time PCR using cerebellum tissues from rats injected 14 days previously with virus or medium. Three animals were used for each group, and each experiment was repeated at least twice. Results of a representative experiment are shown. HPRT, hypoxanthine guanine phosphoribosyl transferase. (C) Protein levels of VEGF were measured by ELISA in supernatants from uninfected BCEC or BCEC infected in vitro with either PVFe5 or PVC-211 MuLV. The presence of viral envelope protein (gp70) in supernatants from BCEC was detected by immunoprecipitation and Western blot analysis. In this experiment, the supernatants were collected at 10 days after infection. The same experiments were repeated at least twice. Results of a representative experiment are shown. All data are means ± standard errors of the means ($P < 0.05$).

be detected as early as 7 dpi, although the difference at that time point was not significant ($P > 0.05$). However, at 14 dpi, a significant difference ($P < 0.05$) in the amount of MIP-1α in the serum was detected between virus-infected rats and controls. By 21 dpi, the levels of MIP-1α in the serum of PVC-211 MuLV-infected rats dropped to control levels. Elevated levels of MIP-1α protein were also detected in the cerebellum and brain stems from PVC-211 MuLV-infected rats compared with control rats at 14 dpi (Fig. 4B), and this was confirmed at the mRNA level by real-time PCR analysis (Fig. 4C).

Since MIP-1α is a monocyte/macrophage chemoattractant, we examined brain tissue from rats infected with PVC-211 MuLV and confirmed activation of microglia by immunostaining with anti-ED-1 antibody. We detected ED-1 by immunofluorescence in the cerebellum and brain stem of PVC-211 MuLV-infected rats at 14 dpi (data not shown), but it was markedly increased at 21 dpi (Fig. 4D). The brains of the control rats were almost free of such staining. As shown in Fig. 4D, ED-1 staining of the cerebellum of PVC-211 MuLV-infected rats occurred only in the cerebellum deep nuclei, where the spongiform neurodegeneration occurs (as verified by the H&E-stained sections), not in the granular layer or molecular layer. ED-1 staining was detected throughout the brain stem (data not shown), whose entire structure is usually affected by spongiform neurodegeneration. These data suggest that increased MIP-1α production in the brains of PVC-211 MuLV-

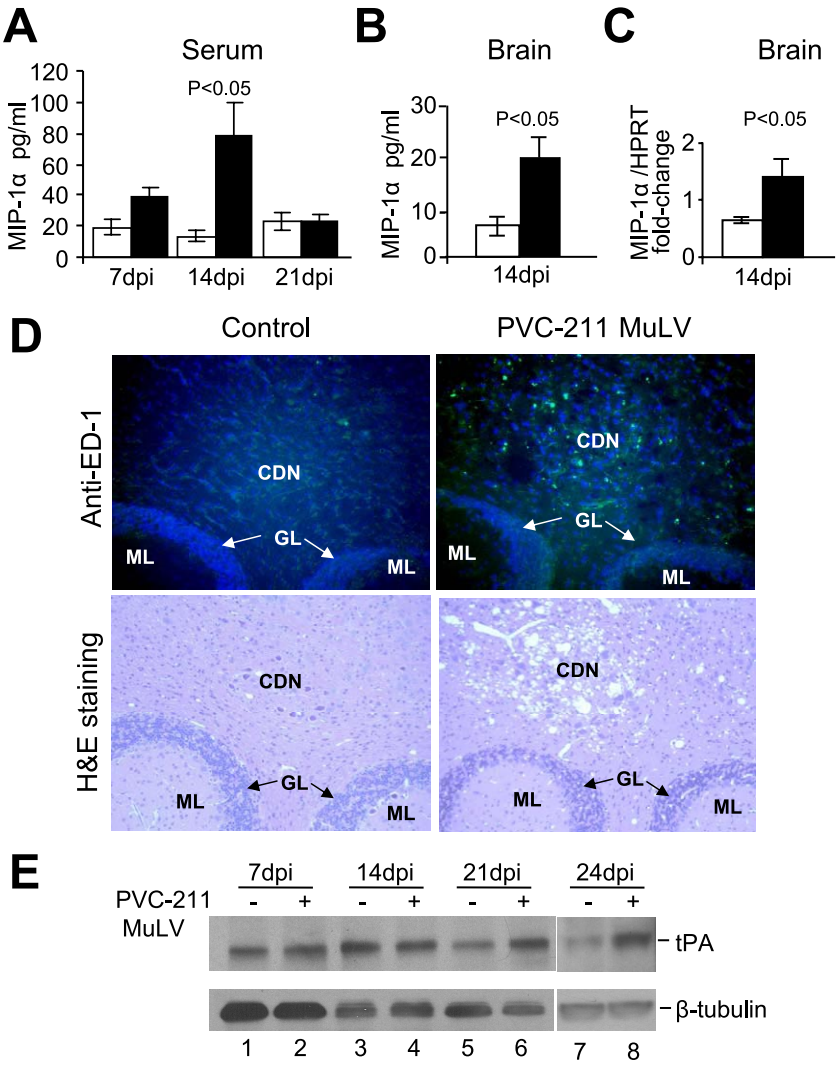

FIG. 4. Increased levels of MIP-1α, activated microglia, and tPA in rats infected with PVC-211 MuLV. (A) MIP-1α levels were detected by ELISA in serum from PVC-211 MuLV-infected and control rats at 7, 14, and 21 dpi. (B) MIP-1α levels were detected by a standard sandwich ELISA in brain tissue (cerebellum and brain stem) from PVC-211 MuLV-infected and control rats at 14 dpi. (C) mRNA levels of MIP-1α were measured by real time PCR using brain tissue (cerebellum and brain stem) from PVC-211 MuLV-infected and control rats at 14 dpi. Three animals were used for each group and each experiment was repeated at least twice. □, control; ■, PVC-211 MuLV; HPRT, hypoxanthine guanine phosphoribosyl transferase. Results of a representative experiment are shown. Data are means ± standard errors of the means. (D) (Top) ED-1 staining (green) of cerebellum from control or PVC-211 MuLV-infected rats at 21 dpi to detect activated microglia. Nuclei are counterstained with DAPI (blue). (Bottom) Similar sections stained with H&E to observe spongiform degeneration. Magnifications, ×20. CDN, cerebellum deep nuclei; GL, granular layer; ML, molecular layer. (E) Western blot analysis of the cerebellum of rats injected 7 to 24 days previously with PVC-211 MuLV or medium with antibodies against tPA or tubulin.

infected rats at 14 dpi may lead to the robust microglial activation at 21 dpi.

Activated microglia in the brain can produce the serine protease tPA, which has been shown to mediate excitotoxin-induced neuronal degeneration (43). To identify whether tPA levels are elevated in the brains of rats infected with PVC-211 MuLV, Western blot analysis was performed with cerebellum and brain stem tissues from virus-infected and control rats. The protein level of tPA in the cerebellums of control rats was highest at 14 dpi (when they were 16 days of age) (Fig. 4E, lane 3), began decreasing at 21 dpi (23 days of age) (lane 5), and was low at 24 dpi (26 days of age) (lane 7), similar to the results in a previous report (49). In the cerebellums from rats infected with PVC-211 MuLV, tPA levels remained high from 14 dpi (Fig. 4E, lane 4) through 21 dpi (lane 6) and 24 dpi (lane 8). This analysis was carried out three separate times, and the difference in tPA levels at 21 and 24 dpi between virus-infected and control rats was consistently detected.

Loss of neurons, demyelination, axonal degeneration and muscle atrophy can be detected in the late stages of the disease induced by PVC-211 MuLV. Previous studies have described the pathological phenotype of PVC-211 MuLV-induced disease as spongiform neurodegeneration occurring in the cerebellum, brain stem, and spinal cord (19). To better understand the events responsible for this phenotype, we examined diseased tissue from PVC-211 MuLV-infected rats specifically for

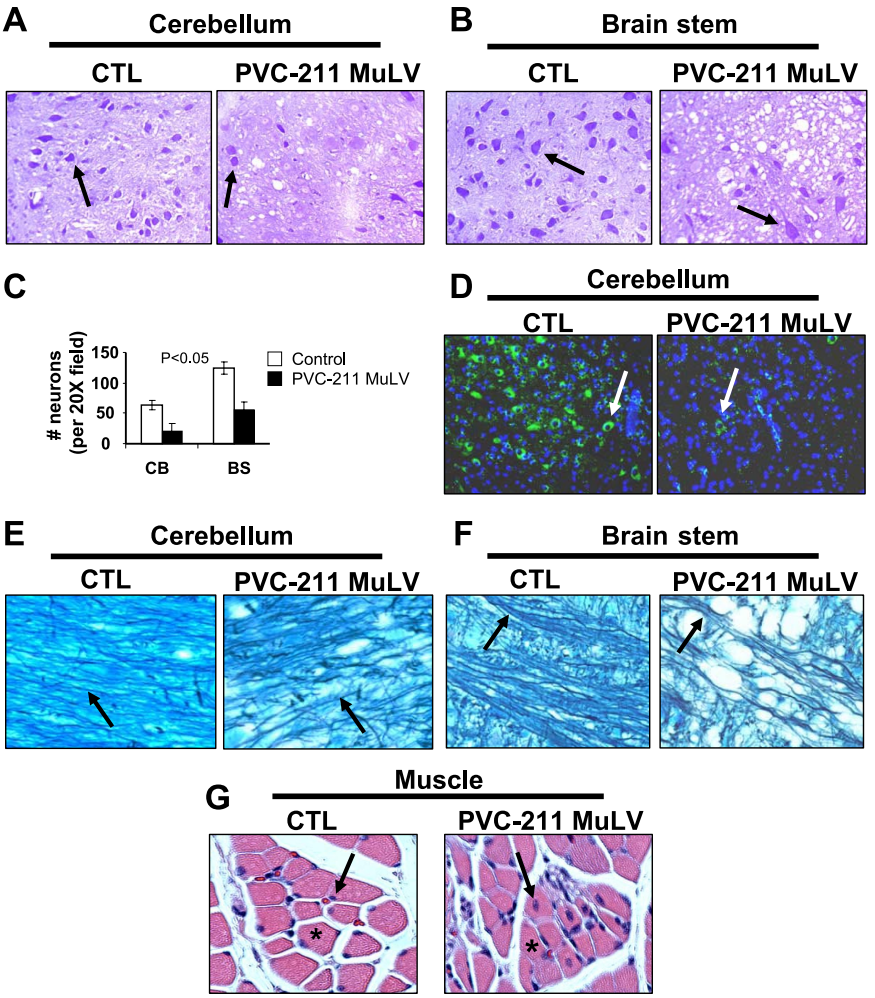

FIG. 5. Loss of neurons, demyelination, and axonal degeneration detected in rats infected with PVC-211 MuLV at 21 dpi. Brain tissues from paralyzed rats infected as newborns with PVC-211 MuLV were compared with tissues from control rats injected with tissue culture medium at 21 dpi. Data are representative of two experiments; three control and three virus-infected rats were examined in each experiment. (A and B) Cresyl violet staining was carried out on sagittal sections of cerebellum and brain stem to identify neurons. Neurons (arrows) appear purple-blue when stained with cresyl violet, as described in Materials and Methods. Magnifications, ×20. (C) Neurons in CV stained sections of cerebellum or brain stem were enumerated; data are means ± standard errors of the means ($P < 0.05$). (D) Immunofluorescence with anti-NSE was assayed on sagittal sections of cerebellum to identify neurons, which stain green (arrows). Nuclei are counterstained with DAPI (blue). Different animals were used for CV and anti-NSE staining. Magnification, ×20. (E and F) Luxol fast blue staining for myelin fibers (arrows) of brain sections from the cerebellum and brain stem. Magnification, ×20. (G) H&E staining of cross-sections of muscle from the lower extremities of the hind limb. Representative muscle fibers are indicated by asterisks; arrows indicate the location of nuclei at the edge of or within muscle fibers. Magnification, ×10.

changes in neurons, myelin, axons, and muscle. Tissues were examined at 7 and 14 dpi as well as when the animals became paralyzed (21 or 24 dpi). No differences were found at the earlier stages of disease (7 dpi), and subtle changes were detected at 14 dpi (data not shown), but obvious changes were observed at the late stage of disease. When stained with cresyl violet, the cerebellums and brain stems (Fig. 5A-C), as well as the spinal cords (data not shown), of diseased areas of paralyzed PVC-211 MuLV-infected rats displayed fewer neurons than the same regions of control rats ($P < 0.05$). These data were confirmed by immunofluorescence staining with an antibody that specifically detects neurons, anti-NSE (Fig. 5D), indicating that loss of neurons occurred in PVC-211 MuLV-infected rats. Signals between neurons and between neurons and muscle are conducted through axons that are surrounded by myelin. To determine whether myelin and axons are involved in the neurological disease, luxol fast blue staining to identify myelin sheaths and axons was performed. Attenuated myelination was found in the spongiform diseased areas of the brains of rats infected with PVC-211 MuLV compared with controls. As shown in Fig. 5E and F, myelin fibers were continuous in the cerebellum and brain stem of control rats but were attenuated and discontinuous in the sections from rats infected with PVC-211 MuLV. Also, the posterior column in the spinal cord, through which axons pass, was smaller in rats infected with PVC-211 MuLV than in control rats (data not shown), suggesting axon degeneration. Damage of lower motor neurons can cause denervation in muscle (muscle atrophy), which oc-

TABLE 1. Neurological disease in PVC-211 MuLV-infected rats treated with clodronate-containing liposomes[a]

Liposomes	No. of rats with				
	Spongiform neurodegeneration severity[b]				Paralysis
	−	+	++	++++	
PBS[c]				3/3	5/5
Clodronate[d]	1/4	1/4	2/4		1/4

[a] Newborn F344 rats were injected i.c. with PBS-containing or clodronate-containing liposomes on day 1. On day 2, rats were injected with PVC-211 MuLV i.c. On days 4 and 7, they were injected again with PBS-liposomes or clodronate-liposomes. Beginning on day 23, they were evaluated for the presence of paralysis, and on day 27, they were euthanized to determine the presence of spongiform neurodegeneration.

[b] Disease severity was determined by measuring the ratio of the area affected by vacuolated lesions compared to the whole brain stem area. −, no detectable pathology; +, spongiform lesions in less than one-quarter of the brainstem; ++, spongiform lesions in less than one-half of the brainstem; ++++, spongiform lesions in more than three-quarters of the brainstem.

[c] A total of five rats were injected, and histological analysis was carried out on three.

[d] A total of six rats were injected. Two died before 23 dpi without paralysis, and histological analysis was carried out on the remaining four.

curs only if the axon itself is damaged. To investigate changes in muscle, we examined histologically the skeletal muscle of the lower extremities of the hind limbs of rats. As shown in Fig. 5G, mild muscle atrophy was detected in paralyzed rats infected with PVC-211 MuLV but not control rats. Homogeneously round muscle fibers with nuclei positioned along the border of the fibers can be seen in the section from the control rat. In contrast, sections from rats infected with PVC-211 MuLV displayed heterogeneous muscle fibers with various sizes and containing nuclei positioned within the muscle fiber (internal nuclei), characteristic of muscle atrophy.

Treatment of PVC-211 MuLV-infected rats with clodronate-containing liposomes blocks microglial activation and causes a significant reduction in neurodegeneration. In order to confirm the role of microglia in the neurodegeneration phenotype, we depleted microglia via intracranial delivery of liposomally encapsulated clodronate. This technique has been previously shown to target only cells of the macrophage lineage (29, 46). As shown in Table 1, all five of the PVC-211 MuLV-infected rats that were treated with PBS-containing liposomes became paralyzed by 27 dpi, while only one of four rats treated with clodronate-containing liposomes became paralyzed (one of the two rats with grade ++ spongiform neurodegeneration). It should be noted that two additional nonparalyzed rats died prematurely (before 23 days of age) from side effects of the clodronate-liposome treatment, which was not reported when clodronate-containing liposomes were given to older rats (15, 38). Histological analysis with H&E staining showed that the spongiform neurodegeneration in the nonparalyzed rats treated with clodronate-containing liposomes was clearly reduced or even absent compared to controls (Fig. 6A). Immunofluorescence staining with ED-1 antibody confirmed that the cerebellum and brain stem of nonparalyzed rats that had been injected with clodronate-containing liposomes had few or no activated microglia compared with rats injected with PBS-liposomes (Fig. 6B). Microglial depletion had no effect on the expression of the virus in the brain tissues, since nonparalyzed rats treated with clodronate-containing liposomes expressed as much MuLV gp70 as rats treated with PBS-containing liposomes (Fig. 6C). These data further support the importance of microglial activation for the development of spongiform neurodegeneration and paralysis induced by PVC-211 MuLV.

DISCUSSION

Although PVC-211 MuLV was shown many years ago to induce spongiform neurodegeneration in rats (24), the precise mechanism by which PVC-211 MuLV causes neurodegeneration is unknown. In the present study, we demonstrate that as early as 2 weeks after PVC-211 MuLV infection, vascular defects can be detected in the areas of the brain that eventually become diseased. This may be the result of increased production of VEGF, which we detect in the cerebellum and brain stem 1 to 2 weeks after virus infection and after in vitro infection of primary BCEC cultures with PVC-211 MuLV. Furthermore, we show that the brains and serum of rats injected 2 weeks previously with PVC-211 MuLV express high levels of the chemokine MIP-1α. Late in the course of disease, when animals are clearly paralyzed, the brains of PVC-211 MuLV-infected rats show loss of neurons, demyelination, axonal degeneration, and muscle atrophy, and brain tissues show elevated levels of tPA, a product of activated microglia that has been implicated in neurodegeneration. Finally, we demonstrate that depletion of microglia from rat brains blocks spongiform neurodegeneration and paralysis induced by PVC-211 MuLV.

VEGF, whose role in vasculogenesis and angiogenesis is well established, was originally discovered and characterized by its ability to increase vascular permeability (40). VEGF has also been shown to enhance permeability in brain vasculature (7, 10), and rats with VEGF infused into the neocortex showed vascular changes similar to those seen in this study (7). The vascular defects observed in the brains of rats infected with PVC-211 MuLV, including increased numbers and sizes of vessels as well as vessel leakage, correlate with the increased level of VEGF detected in brain tissue at an early stage of the disease. Furthermore, purified normal BCEC showed increased VEGF after infection in vitro with PVC-211 MuLV, suggesting that the elevated VEGF expression detected in the diseased brains of virus-infected rats may derive at least in part from PVC-211 MuLV-infected BCEC. Thus, the vascular defects observed in PVC-211 MuLV-infected animals may be directly caused by the increased VEGF. In addition to its effect on vessel structure, VEGF may also play a role in the recruitment and activation of microglia in the brains of PVC-211 MuLV-infected rats. Monocytes/macrophages express receptors for VEGF (39). VEGF has been shown to be a monocyte/macrophage attractant in vitro (18) and when infused into the brains of rats can recruit and activate microglia (7). Furthermore, the vascular defects caused by VEGF, including leakage of vessels, can induce matrix breakdown and loss of cell-cell connection that can be a further stimulus for activation of microglia (26). Hence, changes in VEGF levels and the subsequent vascular defects found in the brains of PVC-211 MuLV-infected rats may be triggers for chemotaxis of microglia to injured areas of the brain. It is unclear how PVC-211 MuLV infection of BCEC results in the elevated expression of VEGF.

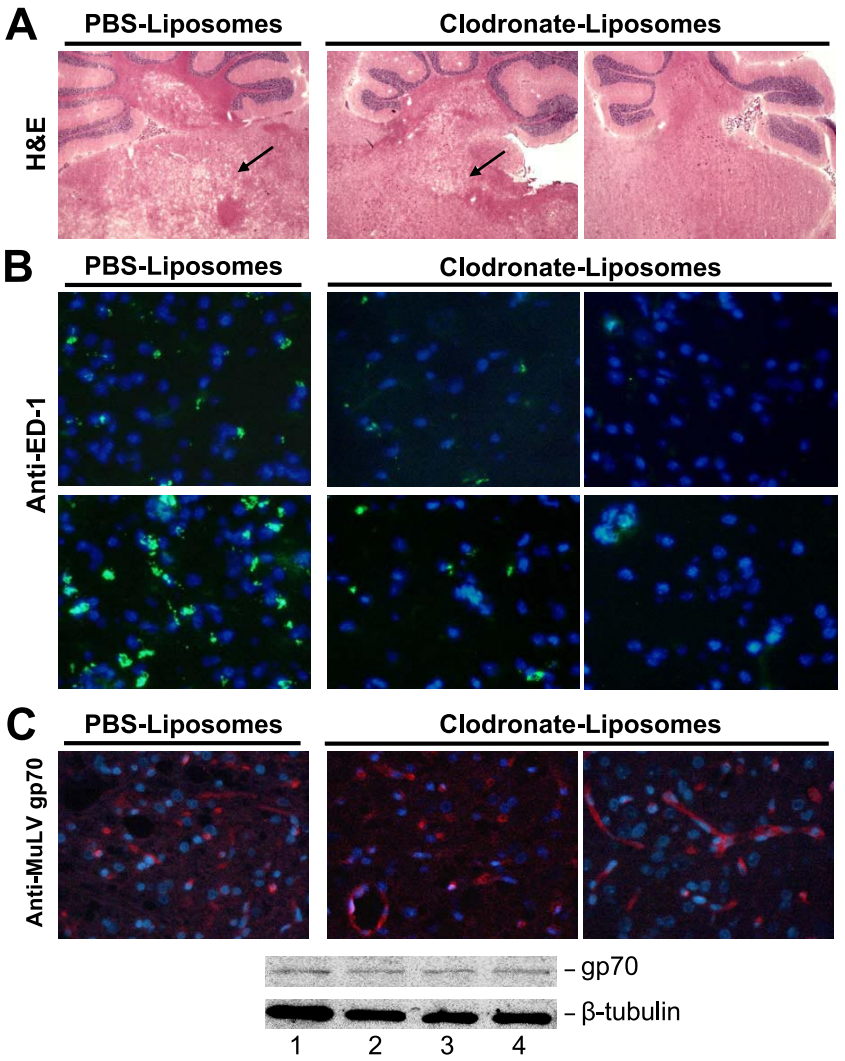

FIG. 6. Reduction in microglial activation and spongiform neurodegeneration in PVC-211 MuLV-infected rats treated with clodronate-containing liposomes. For microglial depletion, newborn rats received i.c. injections of 75 to 100 μl clodronate-containing liposomes or PBS-containing liposomes on days −1, 2, and 5 after injection of PVC-211 MuLV. (A) H&E staining was performed on brain tissues frozen in OCT at 27 dpi of PVC-211 MuLV. Arrows indicate spongiform neurodegeneration. Magnification, ×2. (B) Immunofluorescence with anti-ED-1 was performed using frozen sections of cerebellum (top) and brain stems (bottom). ED-1 staining (green) indicates activated microglia. Nuclei are counterstained with DAPI (blue). Magnification, ×40. (C) Immunofluorescence with anti-MuLV gp70 was carried out to identify the envelope protein of PVC-211 MuLV in brain tissues fixed in paraformaldehyde. Brain stems are shown, but similar results were obtained with cerebellums. Staining with anti-MuLV gp70 (red) indicates envelope protein expression. Nuclei are counterstained with DAPI (blue). Magnification, ×40. Immunofluorescence data were confirmed by Western blot analysis for MuLV gp70 using brain stems from PVC-211 MuLV-infected rats injected with PBS-containing liposomes (lanes 1 and 2) or clodronate-containing liposomes (lanes 3 and 4). Antitubulin was used as a loading control.

Consistent with our observations, there is mounting evidence from a number of models that cytokines and chemokines released from hyperactivation of microglia are involved in neuron damage (6, 7, 26), although different molecules may be involved in different neurodegenerative diseases. For example, in a rat model for acute stroke, increased MCP-1, IL-1β, and CINC-1 were associated with activated microglia prior to neuronal damage (8). Mice infected with the neurovirulent MuLV FrCasE showed increased levels of MIP-1α and MIP-1β early in the course of disease (3), while mice infected with the neurovirulent polytropic MuLV Fr98 showed increased expression of TNF-α, TNF-β, IL-1α, MIP-1α, MIP-1β, MCP-1, IP10, and RANTES (37). In our study, MIP-1α was elevated in the brains of PVC-211 MuLV-infected rats. MIP-1α expression peaks earlier than the peak of activated microglia detected by ED-1 staining, supporting the idea that MIP-1α may lead to microglial invasion (3, 13, 35). Early expression of MIP-1α has been implicated in the switch of recruited cells from polymorphonuclear monocytes to macrophages at the site of insult (13, 35). Thus, recruitment of microglia by MIP-1α might play a key role in the development of neurodegeneration induced by PVC-211 MuLV. This idea is consistent with a previous study showing that deletion of the MIP-1α gene retards neurodegeneration in a mouse model (48).

Many different cytokines and chemokines can be secreted from activated microglia, but among the 13 tested for in our

preliminary screen, the only one that was clearly elevated in the brains of PVC-211 MuLV-infected rats early in the course of disease was MIP-1α. This result suggests that the production of MIP-1α may be specifically influenced by VEGF. Interestingly, both MIP-1α and VEGF have been found to be increased after corneal damage (35), and MIP-1α has been found to be elevated in some human (20) and animal (7) models of neurological diseases related to vascular permeability. Infusion of VEGF into the brains of adult rats results in the specific upregulation of MIP-1α but not other chemokines, such as MCP-1, RANTES, and GROα (MIP-2α) (7). Also, vascular damage induced in the cornea by chemical cauterization not only activates VEGF but also specifically activates MIP-1α and not inflammatory cytokines, such as TNF-α (35). These data suggest that VEGF may directly or indirectly initiate a specific increase in MIP-1α. However, in our model we cannot exclude other possibilities, including that PVC-211 MuLV infection of BCEC may produce other factors that affect the production of MIP-1α and that this can further stimulate microglia to produce more MIP-1α.

Although primary BCEC infected in vitro with PVC-211 MuLV produce elevated levels of VEGF, they do not produce MIP-1α (data not shown), suggesting that other cells within the CNS, such as microglia, are the source of this chemokine. Microglia have been shown to contribute to a number of human neurodegenerative diseases, including Alzheimer's, human immunodeficiency virus dementia, multiple sclerosis, and others (6, 12, 26). However, the role of activated microglia in retrovirus-induced animal models of neurodegeneration has been controversial (16, 28). At least three lines of evidence support the idea that microglia may be involved in the spongiform neurodegeneration induced by PVC-211 MuLV. First of all, we and others (47) have detected a marked accumulation of activated microglia (microgliosis) as early as 14 dpi in the regions of PVC-211 MuLV-infected rats that are rich in spongiform neurodegeneration at 21 dpi, suggesting that microgliosis might be a prerequisite for inducing spongiform neurodegeneration. Second, MIP-1α, a chemokine originally reported to be involved in macrophage recruitment (9, 30), is increased at the early stage of PVC-211 MuLV-induced disease, beginning at 7 dpi and peaking at 14 dpi, and may recruit macrophages and/or microglia to the brain. Finally, treatment of PVC-211 MuLV-infected rats with clodronate-containing liposomes, which specifically kill macrophages and microglia, causes a significant inhibition of neurodegeneration and paralysis. To ensure sufficient activation of microglia in our virus-induced model of neurodegeneration, two possible phases may need to be coordinated. At the early stage of PVC-211 MuLV-induced disease, microglia may be activated by many factors, such as exposure to viral antigens or increased VEGF and/or leakage of vessels. The activated microglia may then be recruited by chemokines (i.e., MIP-1α) to the areas of the brain that eventually become diseased. Factors secreted from the activated microglia at this time, such as NO, may cause some neuron damage, but a certain concentration of neurotoxic factors may be needed to cause severe enough spongiform neurodegeneration to result in paralysis. Additional neurotoxic factors may come from the BCEC of PVC-211 MuLV-infected rats, which have been shown to express high levels of iNOS (23), leading to higher levels of NO. Late in the course of the disease, additional numbers of microglia may be activated in response to degeneration of neurons, producing even more neurotoxic factors. The accumulation of high numbers of activated microglia may further be responsible for the high level of tPA, which has been shown to be associated with neuronal degeneration (2, 42, 43), and this may result in progressively advanced neurological disease in a short period of time.

In the present study, we have better defined the pathological phenotype of neurodegeneration induced by PVC-211 MuLV by demonstrating not only the loss of neurons but also demyelination, axonal degeneration, and muscle atrophy. These changes may be triggered by a common factor, such as activation of microglia, and progress together. Alternatively, they may be unlinked events. Which event is the most important for the development of paralysis in our model is not known. Degeneration of axons is not likely the main cause of paralysis, since the muscle atrophy observed in PVC-211 MuLV-infected rats is very mild compared to that found in some other models of neurodegeneration (44). Since demyelination can induce paralysis in human multiple sclerosis (4, 17) and in animal models (25), the severe demyelination observed in PVC-211 MuLV rats, combined with the loss of neurons, may be the main cause of paralysis.

In summary, PVC-211 MuLV infects BCEC and alters VEGF expression by an unknown pathway to initiate neurological disease. Although neurons may be directly damaged by factors secreted from infected BCEC, such as NO, our results demonstrate that neuronal damage requires activation of an indirect pathway that involves microglial activation. Our studies using microglial depletion clearly demonstrate the importance of activated microglia in the development of PVC-211 MuLV-induced spongiform neurodegeneration. Since depleting microglia can have lethal side effects, we have initiated studies to assess the effects of blocking MIP-1α and/or VEGF, both of which appear to lead to activation of microglia. We are also testing the effects of tPA inhibition on the severity of the neurodegeneration induced by PVC-211 MuLV. Since VEGF, chemokines, and tPA appear to be involved in many human neurological diseases, including human immunodeficiency virus-associated dementia, multiple sclerosis, and stroke (14, 34, 36, 41), our studies with PVC-211 MuLV may provide useful preclinical information about the efficacy of targeting these molecules to treat neurodegenerative diseases.

ACKNOWLEDGMENTS

This work was supported by the Intramural Research Program of the National Institutes of Health, National Cancer Institute, Center for Cancer Research.

We thank Peter Kaczmarek for his generosity in helping us to prepare clodronate-containing liposomes. We also thank Chris Perella for excellent technical assistance with our animal studies.

REFERENCES

1. **Ajuebor, M. N., C. M. Hogaboam, T. Le, A. E. Proudfoot, and M. G. Swain.** 2004. CCL3/MIP-1α is pro-inflammatory in murine T cell-mediated hepatitis by recruiting CCR1-expressing $CD4^+$ T cells to the liver. Eur. J. Immunol. **34:**2907–2918.
2. **Armstead, W. M., T. Nassar, S. Akkawi, D. H. Smith, X. H. Chen, D. B. Cines, and A. A. Higazi.** 2006. Neutralizing the neurotoxic effects of exogenous and endogenous tPA. Nat. Neurosci. **9:**1150–1155.
3. **Askovic, S., C. Favara, F. J. McAtee, and J. L. Portis.** 2001. Increased expression of MIP-1α and MIP-1β mRNAs in the brain correlates spatially and temporally with the spongiform neurodegeneration induced by a murine oncornavirus. J. Virol. **75:**2665–2674.

4. **Beeton, C., A. Garcia, and K. G. Chandy.** 2007. Induction and clinical scoring of chronic-relapsing experimental autoimmune encephalomyelitis. J. Vis. Exp. **5:**224.
5. **Blease, K., B. Mehrad, N. W. Lukacs, S. L. Kunkel, T. J. Standiford, and C. M. Hogaboam.** 2001. Antifungal and airway remodeling roles for murine monocyte chemoattractant protein-1/CCL2 during pulmonary exposure to Aspergillus fumigatus conidia. J. Immunol. **166:**1832–1842.
6. **Block, M. L., L. Zecca, and J. S. Hong.** 2007. Microglia-mediated neurotoxicity: uncovering the molecular mechanisms. Nat. Rev. Neurosci. **8:**57–69.
7. **Croll, S. D., R. M. Ransohoff, N. Cai, Q. Zhang, F. J. Martin, T. Wei, L. J. Kasselman, J. Kintner, A. J. Murphy, G. D. Yancopoulos, and S. J. Wiegand.** 2004. VEGF-mediated inflammation precedes angiogenesis in adult brain. Exp. Neurol. **187:**388–402.
8. **Denker, S. P., S. Ji, A. Dingman, S. Y. Lee, N. Derugin, M. F. Wendland, and Z. S. Vexler.** 2007. Macrophages are comprised of resident brain microglia not infiltrating peripheral monocytes acutely after neonatal stroke. J. Neurochem. **100:**893–904.
9. **DiPietro, L. A., M. Burdick, Q. E. Low, S. L. Kunkel, and R. M. Strieter.** 1998. MIP-1α as a critical macrophage chemoattractant in murine wound repair. J. Clin. Investig. **101:**1693–1698.
10. **Dobrogowska, D. H., A. S. Lossinsky, M. Tarnawski, and A. W. Vorbrodt.** 1998. Increased blood-brain barrier permeability and endothelial abnormalities induced by vascular endothelial growth factor. J. Neurocytol. **27:**163–173.
11. **Fetler, L., and S. Amigorena.** 2005. Neuroscience. Brain under surveillance: the microglia patrol. Science **309:**392–393.
12. **Fischer-Smith, T., S. Croul, A. Adeniyi, K. Rybicka, S. Morgello, K. Khalili, and J. Rappaport.** 2004. Macrophage/microglial accumulation and proliferating cell nuclear antigen expression in the central nervous system in human immunodeficiency virus encephalopathy. Am. J. Pathol. **164:**2089–2099.
13. **Gourmala, N. G., S. Limonta, D. Bochelen, A. Sauter, and H. W. Boddeke.** 1999. Localization of macrophage inflammatory protein: macrophage inflammatory protein-1 expression in rat brain after peripheral administration of lipopolysaccharide and focal cerebral ischemia. Neuroscience **88:**1255–1266.
14. **Gravanis, I., and S. E. Tsirka.** 2008. Tissue-type plasminogen activator as a therapeutic target in stroke. Expert Opin. Ther. Targets **12:**159–170.
15. **Gray, M., W. Palispis, P. G. Popovich, N. van Rooijen, and R. Gupta.** 2007. Macrophage depletion alters the blood-nerve barrier without affecting Schwann cell function after neural injury. J. Neurosci. Res. **85:**766–777.
16. **Hansen, R., C. Sauder, S. Czub, E. Bachmann, S. Schimmer, A. Hegyi, and M. Czub.** 2001. Activation of microglia cells is dispensable for the induction of rat retroviral spongiform encephalopathy. J. Neurovirol. **7:**501–510.
17. **Hauser, S. L., and J. R. Oksenberg.** 2006. The neurobiology of multiple sclerosis: genes, inflammation, and neurodegeneration. Neuron **52:**61–76.
18. **Heil, M., M. Clauss, K. Suzuki, I. R. Buschmann, A. Willuweit, S. Fischer, and W. Schaper.** 2000. Vascular endothelial growth factor (VEGF) stimulates monocyte migration through endothelial monolayers via increased integrin expression. Eur. J. Cell Biol. **79:**850–857.
19. **Hoffman, P. M., E. F. Cimino, D. S. Robbins, R. D. Broadwell, J. M. Powers, and S. K. Ruscetti.** 1992. Cellular tropism and localization in the rodent nervous system of a neuropathogenic variant of Friend murine leukemia virus. Lab. Investig. **67:**314–321.
20. **Iadecola, C.** 2004. Neurovascular regulation in the normal brain and in Alzheimer's disease. Nat. Rev. Neurosci. **5:**347–360.
21. **Inai, T., M. Mancuso, H. Hashizume, F. Baffert, A. Haskell, P. Baluk, D. D. Hu-Lowe, D. R Shalinsky, G. Thurston, G. D. Yancopoulos, and D. M. McDonald.** 2004. Inhibition of vascular endothelial growth factor (VEGF) signaling in cancer causes loss of endothelial fenestrations, regression of tumor vessels, and appearance of basement membrane ghosts. Am. J. Pathol. **165:**35–52.
22. **Jinno-Oue, A., M. Oue, and S. K. Ruscetti.** 2001. A unique heparin-binding domain in the envelope protein of the neuropathogenic PVC-211 murine leukemia virus may contribute to its brain capillary endothelial cell tropism. J. Virol. **75:**12439–12445.
23. **Jinno-Oue, A., S. G. Wilt, C. Hanson, N. V. Dugger, P. M. Hoffman, M. Masuda, and S. K. Ruscetti.** 2003. Expression of inducible nitric oxide synthase and elevation of tyrosine nitration of a 32-kilodalton cellular protein in brain capillary endothelial cells from rats infected with a neuropathogenic murine leukemia virus. J. Virol. **308:**1314–1318.
24. **Kai, K., and T. Furuta.** 1984. Isolation of paralysis-inducing murine leukemia viruses from Friend virus passaged in rats. J. Virol. **50:**970–973.
25. **Kuramoto, T., K. Kitada, T. Inui, Y. Sasaki, K. Ito, T. Hase, S. Kawagachi, Y. Ogawa, K. Nakao, G. S. Barsh, M. Nagao, T. Ushijima, and T. Serikawa.** 2001. Attractin/mahogany/zitter plays a critical role in myelination of the central nervous system. Proc. Natl. Acad. Sci. USA **98:**559–564.
26. **Langmann, T.** 2007. Microglia activation in retinal degeneration. J. Leukoc. Biol. **81:**1345–1351.
27. **Li, X., E. Calvo, M. Cool, P. Chrobak, D. G. Kay, and P. Jolicoeur.** 2007. Overexpression of Notch1 ectodomain in myeloid cells induces vascular malformations through a paracrine pathway. Am. J. Pathol. **170:**399–415.
28. **Lynch, W. P., S. J. Robertson, and J. L. Portis.** 1995. Induction of focal spongiform neurodegeneration in developmentally resistant mice by implantation of murine retrovirus-infected microglia. J. Virol. **69:**1408–1419.
29. **Marín-Teva, J. L., I. Dusart, C. Colin, A. Gervais, N. van Rooijen, and M. Mallat.** 2004. Microglia promote the death of developing Purkinje cells. Neuron **41:**535–547.
30. **Marshall, E., L. B. Woolford, and B. I. Lord.** 1997. Continuous infusion of macrophage inflammatory protein MIP-1α enhances leucocyte recovery and haemopoietic progenitor cell mobilization after cyclophosphamide. Br. J. Cancer **75:**1715–1720.
31. **Masuda, M., C. A. Hanson, W. G. Alvord, P. M. Hoffman, S. K. Ruscetti, and M. Masuda.** 1996. Effects of subtle changes in the SU protein of ecotropic murine leukemia virus on its brain capillary endothelial cell tropism and interference properties. Virology **215:**142–151.
32. **Masuda, M., P. M. Hoffman, and S. K. Ruscetti.** 1993. Viral determinants that control the neuropathogenicity of PVC-211 murine leukemia virus in vivo determine brain capillary endothelial cell tropism of the virus in vitro. J. Virol. **67:**4580–4587.
33. **Masuda, M., M. P. Remington, P. M. Hoffman, and S. K. Ruscetti.** 1992. Molecular characterization of a neuropathogenic and nonerythroleukemogenic variant of Friend murine leukemia virus PVC-211. J. Virol. **66:**2798–2806.
34. **Mines, M., Y. Ding, and G. H. Fan.** 2007. The many roles of chemokine receptors in neurodegenerative disorders: emerging new therapeutic strategies. Curr. Med. Chem. **14:**2456–2470.
35. **Ogawa, S., S. Yoshida, M. Ono, H. Onoue, Y. Ito, T. Ishibashi, H. Inomata, and M. Kuwano.** 1999. Induction of macrophage inflammatory protein-1α and vascular endothelial growth factor during inflammatory neovascularization in the mouse cornea. Angiogenesis **3:**327–334.
36. **Persidsky, Y., M. Buttini, J. Limoges, P. Bock, and H. E. Gendelman.** 1997. An analysis of HIV-1-associated inflammatory products in brain tissue of humans and SCID mice with HIV-1 encephalitis. J. Neurovirol. **3:**401–416.
37. **Peterson, K. E., S. J. Robertson, J. L. Portis, and B. Chesebro.** 2001. Differences in cytokine and chemokine responses during neurological disease induced by polytropic murine retroviruses map to separate regions of the viral envelope gene. J. Virol. **75:**2848–2856.
38. **Popovich, P. G., Z. Guan, P. Wei, I. Huitinga, N. van Rooijen, and B. T. Stokes.** 1999. Depletion of hematogenous macrophages promotes partial hindlimb recovery and neuroanatomical repair after experimental spinal cord injury. Exp. Neurol. **158:**351–365.
39. **Sawano, A., S. Iwai, Y. Sakurai, M. Ito, K. Shitara, T. Nakahata, and M. Shibuya.** 2001. Flt-1, vascular endothelial growth factor receptor 1, is a novel cell surface marker for the lineage of monocyte-macrophages in humans. Blood **97:**785–791.
40. **Senger, D. R., C. A. Perruzzi, J. Feder, and H. F. Dvorak.** 1986. A highly conserved vascular permeability factor secreted by a variety of human and rodent tumor cell lines. Cancer Res. **46:**5629–5632.
41. **Szczuciński, A., and J. Losy.** 2007. Chemokines and chemokine receptors in multiple sclerosis. Potential targets for new therapies. Acta Neurol. Scand. **115:**137–146.
42. **Teesalu, T., A. Kulla, T. Asser, M. Koskiniemi, and A. Vaheri.** 2002. Tissue plasminogen activator as a key effector in neurobiology and neuropathology. Biochem. Soc. Trans. **30:**183–189.
43. **Tsirka, S. E., A. Gualandris, D. G. Amaral, and S. Strickland.** 1995. Excitotoxin-induced neuronal degeneration and seizure are mediated by tissue plasminogen activator. Nature **377:**340–344.
44. **Tsunoda, I., T. Tanaka, E. J. Terry, and R. S. Fujinami.** 2007. Contrasting roles for axonal degeneration in an autoimmune versus viral model of multiple sclerosis: when can axonal injury be beneficial? Am. J. Pathol. **170:**214–226.
45. **Van Rooijen, N., and A. Sanders.** 1994. Liposome mediated depletion of macrophages: mechanism of action, preparation of liposomes and applications. J. Immunol. Methods **174:**83–93.
46. **van Rooijen, N., A. Sanders, and T. K. van den Berg.** 1996. Apoptosis of macrophages induced by liposome-mediated intracellular delivery of clodronate and propamidine. J. Immunol. Methods **193:**93–99.
47. **Wilt, S. G., N. V. Dugger, N. D. Hitt, and P. M. Hoffman.** 2000. Evidence for oxidative damage in a murine leukemia virus-induced neurodegeneration. J. Neurosci. Res. **62:**440–450.
48. **Wu, Y. P., and R. L. Proia.** 2004. Deletion of macrophage-inflammatory protein 1 alpha retards neurodegeneration in Sandhoff disease mice. Proc. Natl. Acad. Sci. USA **101:**8425–8430.
49. **Zheng, S., Z. Q. Yin, and Y. X. Zeng.** 2008. Developmental profile of tissue plasminogen activator in postnatal Long Evans rat visual cortex. Mol. Vis. **14:**975–982.